Relative Experimental Cross Sections for Excitation of Ba^+ Ions by Electron Impact (8.0–98 eV)*

F. M. Bacon† and J. W. Hooper
School of Electrical Engineering, Georgia Institute of Technology, Atlanta, Georgia
(Received 2 August, 1968)

A crossed beam technique has been developed for measuring the emission cross section for the excitation of electric dipole transitions in ions by electron impact. The experimental method involves crossing modulated ion and electron beams in a well-defined collision volume. A portion of the photon flux radiated from the excited ions is detected at an angle of 90° to the plane of the two beams by direct observation of the collision volume with a photomultiplier tube. The selection of a single emission line is accomplished with an interference filter. The total flux of radiation from the collision volume for a particular transition can be determined with a knowledge of the photon detection probability of the apparatus. The possibility of an anisotropic angular distribution of radiation from the collision volume is evaluated by measuring the polarization fraction. The emission cross section can be determined from the ion and electron beam currents, current density distributions and energies, and the total radiation flux.

This technique has been used to measure the relative emission cross sections for excitation of the resonance transitions in Ba^+ ions by electron impact. The resonance transitions, between the excited $6^2P_{1/2}^\circ$ and $6^2P_{3/2}^\circ$ levels and the $6^2S_{1/2}$ ground state, produce photons with wavelengths of 4934 and 4554 Å. The thresholds for exciting the $6^2P_{1/2}^\circ$ and $6^2P_{3/2}^\circ$ levels are 2.5 and 2.7 eV, respectively. Over the energy range of the experiment, from 8 to 98 eV, the relative cross sections differ by approximately a factor of two, the ratio of the statistical weights of the $6P$ levels. The relative data also exhibit the high energy dependence predicted by the Bethe-Born approximation. From a best estimate of the photon detection probability of the apparatus, estimated absolute cross sections are obtained which agree remarkably well in magnitude and shape with the theoretical predictions. Checks on the data were performed to evaluate the possible effects of such parameters as the beam intensities, beam modulation frequency, ion beam composition, ion beam energy, electron beam energy distribution, beam profiles, and signal-to-noise ratio.

I. INTRODUCTION

A crossed-beam technique has been developed to determine the emission cross sections for the excitation of the resonance transitions of Ba^+ ions by electron impact over the energy range from 8 to 98 eV.[1] The process can be described by the following equations:

$$e + Ba^+ \rightarrow e + (Ba^+)^*, \quad (Ba^+)^* \rightarrow Ba^+ + \text{photon}. \quad (1)$$

As shown in the energy level diagram[2] in Fig. 1, the resonance transitions occur between the $6^2P_{1/2}^\circ$ and $6^2P_{3/2}^\circ$ levels and the $6^2S_{1/2}$ level with wavelengths of 4934 and 4554 Å. The thresholds for exciting the $6^2P_{1/2}^\circ$ and $6^2P_{3/2}^\circ$ levels are 2.5 and 2.7 eV, respectively.

The experimental method involves crossing modulated ion and electron beams in a well-defined collision volume. After the ion is excited by collision with an electron, the electric dipole transitions occur before the ion has traveled a millimeter because the lifetimes of the excited states of interest are approximately[3] 10^{-8} sec and the velocity of the ions is approximately 10^6 centimeters per second. A portion of the radiation from the excited ions is detected by direct observation of the interaction region with a photomultiplier tube operated in a counting mode. The selection of a single resonance line is made with an interference filter. With a knowledge of the photon detection probability and the photon flux angular distribution around the collision volume, the magnitude of the cross sections is determined.

The present results represent the first measurement of an emission cross section for the excitation of electric dipole transitions in an ion by electron impact using crossed beam techniques. Since the first report of this work,[4] similar measurements have been made[5] in N_2^+. The development of this measurement technique was the principal motivation for performing the experiment. A practical incentive for obtaining information on the excitation of barium ions by electron impact

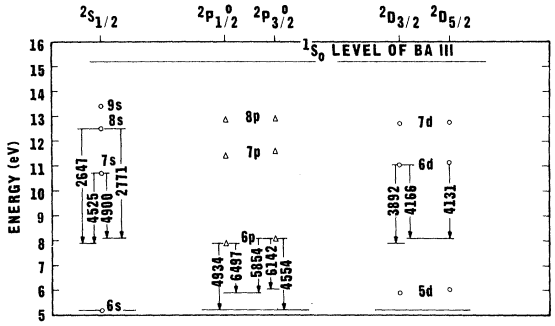

FIG. 1. Energy level diagram of Ba^+.

is related to the use of barium in studies of quiescent plasmas in the controlled thermonuclear research program.[6]

Several electron-ion crossed beam experiments have been successfully completed since the work of Dolder, Harrison, and Thonemann[7] in 1961. Discussions of the experimental technique and associated problems are presented by several authors.[8–10]

The experiment of Dance, Harrison, and Smith[11] on the excitation of the 2S level of He^+ by electron impact represents the only electron-ion crossed beam measurement of an emission cross section completed prior to the present work. It should be noted, however, that there is a basic difference between the work of Dance, *et. al.*, and the present results on the excitation of Ba^+. The 2S level examined in their experiment is metastable, and consequently, observation of the desired transitions may be made in a quench field located a sufficient distance downstream from the interaction region to permit the decay of the ordinary excited states before the ions reach the quench region. Such a technique appears possible only for hydrogenic structures which have ordinary excited levels lying very close to the metastable levels. The application of an electric field to such excited ions can lead to sufficient overlap of the wave functions of the metastable and optically permitted levels to permit quenching of the metastable state. In contrast, direct observation in or near the interaction region is required in the study of ordinary excited ions.

II. EXPERIMENTAL TECHNIQUE

Consider a monoenergetic, singly ionized, ion beam and a monoenergetic electron beam traveling parallel to the X and Y axes, respectively, of a rectangular coordinate system. Let V_i and V_e be the ion and electron velocities. If both beams are sufficiently tenuous that multiple collisions can be neglected, then the cross section for production of electric dipole radiation by ion-electron impact can be shown[1, 8–10] to be

$$\sigma_{em} = \Phi_T \frac{e^2 V_i V_e}{(V_i^2 + V_e^2)^{1/2}} \frac{F}{I_i I_e}, \tag{2}$$

$$\text{where } F = \frac{\int_{-\infty}^{\infty} i_i(z)dz \int_{-\infty}^{\infty} i_e(z)dz}{\int_{-\infty}^{\infty} i_i(z) i_e(z)dz}, \tag{3}$$

Φ_T is the total flux of photons (photons/second) emitted from the collision volume, I_i is the total ion beam current, I_e is the total electron beam current, e is the magnitude of the electronic charge, and $i_i(z)dz$ and $i_e(z)dz$ are the ion and electron currents passing through the region z to $z+dz$.

The cross section in Eq. (2), σ_{em}, is defined as an emission cross section because the process described by Eq. (1) results in the emission of a photon. Actually, as indicated by Eq. (1), the emission cross section represents a two-step process: the excitation of a given level and then the decay of that excited state by the emission of a photon. The emission cross section contains cascading contributions from higher energy levels to the 6^2P levels. In the case of Ba^+, the $6^2P \rightarrow 5^2D$ transitions compete with the resonance transitions for the depopulation of the 6^2P levels.

Radiation emitted as a result of particle impact often exhibits polarization effects[12] determined by the direction of the particle beam which produces the excitation. Let $\phi_{\parallel}$ and $\phi_{\perp}$ be the photon fluxes observed at an angle of 90° to the exciting beam with electric vectors parallel and perpendicular to the direction of the exciting beam, respectively. Then the polarization fraction P is defined as

$$P = (\phi_{\parallel} - \phi_{\perp})/(\phi_{\parallel} + \phi_{\perp}). \tag{4}$$

In electric dipole radiation, the angular distribution of the radiation flux is given by the equation

$$\phi(\theta) = (\Phi_T/4\pi)\, 3(1 - P\cos^2\theta)/(3 - P), \tag{5}$$

where $\phi(\theta)$ is the photon flux per unit solid angle emitted in the direction between θ and $\theta + d\theta$, and Φ_T is the total flux. The angle θ is measured with respect to the exciting beam, in this case, the electron beam.

Only a fraction of the total flux from the collision volume is detected by the photomultiplier tube centered on the Z axis or $\theta = 90°$. If the photon detection probability is η, then the signal S from the detection system is given by

$$S = 4\pi\phi(90°)\eta = [3\eta/(3 - P)]\,\Phi_T. \tag{6}$$

Solving this equation for Φ_T and substituting into Eq. (2) gives the emission cross section in terms of the experimentally observable quantities:

$$\sigma_{em} = \frac{S}{\eta} \frac{3 - P}{3} \frac{e^2 V_i V_e}{(V_i^2 + V_e^2)^{1/2}} \frac{F}{I_i I_e}. \tag{7}$$

The program for the experimental determination of σ_{em} was (1) measurement of the relative cross section expressed as

$$\sigma_{em}^R = \frac{3\eta}{3 - P}\sigma_{em} = \frac{S}{I_i} \frac{F}{I_e} \frac{e^2 V_i V_e}{(V_i^2 + V_e^2)^{1/2}}, \tag{8}$$

(2) measurement of the polarization fraction P, and (3) evaluation of the photon detection probability η.

The parameters in Eq. (8) most difficult to determine accurately are the form factor F and the signal S. The form factor is evaluated by scanning both beams simultaneously using an L-shaped probe with coplanar slits similar to those used by others.[7, 9–11] An alternative procedure for obtaining F utilizes the top of the probe to measure the integral of the current distributions. Differentiation of the resulting data then gives the distribution functions $i_i(z)$ and $i_e(z)$. As Dunn and

Van Zyl[10] have discussed, equivalence of the two methods is taken as evidence that possible errors resulting from differences in space charge due to probe positions, possible image charges on the probe, or insulating layers on the probe surface are not important. The possibility of errors in measuring F decreases with increasing uniformity of the ion beam, if the electron beam is well contained inside the ion beam. These constraints allow for space-charge expansion of the electron beam as it travels through the interaction region, and also for the possibility that the axis of the electron beam may be slightly nonparallel to the Y axis. The slit scanner technique has been carefully evaluated by Dunn and Van Zyl even without the above constraints on the beams, and, under their operating conditions, was shown to be accurate to $\pm 1\%$. Since F could not be varied over a significant range in the present experiment, the precaution was taken to maintain the electron beam inside a uniform ion beam.

The evaluation of S would be simple were it not for sources of photons of wavelengths identical to, or approximately equal to, those of the signal. This flux of photons, identified here as noise, is often a factor of 100 times the signal. An effective method for extracting the signal from this noise is the double beam modulation system described in the following section.

In this crossed beam experiment the electron velocity V_e is much greater than the ion velocity V_i. Under this condition the relative velocity of an ion and an electron is essentially the electron velocity; therefore, the total energy in the center-of-mass reference frame is very nearly equal to the laboratory energy of the electron. Since the cross section should be a function only of the total center-of-mass energy, the measured cross sections should remain constant as the ion energy is varied, provided that the electron energy is fixed. For a given electron energy the measured cross sections should be independent of changes in the electron beam intensity, the ion beam intensity, and the form factor F. The variation of each of the parameters in Eq. (8) provides a valuable check on some aspects of the performance of the experimental apparatus. The results must also be independent of other experimental parameters not contained in this equation, such as the beam modulation frequency and the magnitude of the noise.

The polarization fraction P is determined from the measurement of $\phi_{\parallel}$ and $\phi_{\perp}$ by introducing a polarizing film between the collision volume and the photomultiplier tube, so that the polarizing axis is first parallel and then perpendicular to the direction of the electron beam. The finite solid angle at $\theta = 90°$ subtended by the detection system gives a value of P that is less than the theoretical P, which is evaluated at $\theta = 90°$ and zero solid angle. Since the signal is measured with this same finite solid angle, the measured value of P is the proper value to use when correcting for the anisotropy in the photon flux distribution introduced by the polarization.

To obtain an absolute cross section, the photon detection probability η can, in principle, be measured by determining the response of the experimental system to a source of known luminosity, such as a blackbody radiator. No such direct calibration is made in the present work; instead, the photon detection probability is estimated by evaluating the solid angle subtended by the detection system and estimating the transmission of the windows and filters and the quantum efficiency of the photomultiplier tube from manufacturer's data. The results are termed an "estimated absolute cross section," thereby reserving the term "absolute cross section" for those cases where the calibration is determined by proper standards.

III. EXPERIMENTAL APPARATUS

A schematic diagram of the experimental apparatus is presented in Fig. 2. In the diagram the slit scanner is shown in position for scanning the beams; during measurement of parameters other than the form factor, the scanner was raised out of the interaction region. The apparatus used for producing and collecting the ion and electron beams is attached to an experiment plate which is bolted to the top cover of a vacuum chamber. This apparatus is then suspended inside the vacuum chamber which is evacuated to pressures of the order of 10^{-9} Torr. The current measuring apparatus and the photon detection system are located outside the vacuum chamber. A viewing port in the chamber cover permits the direct observation of the beam interaction region.

A. Vacuum System

The vacuum enclosure is an all stainless steel bakable chamber 21 inches in diameter by 6 inches deep. Most of the vacuum seals are metal O-ring compression seals using soft aluminum wire; the flange around the viewing port is a Varian "Conflat" flange. The pumping system consists of a

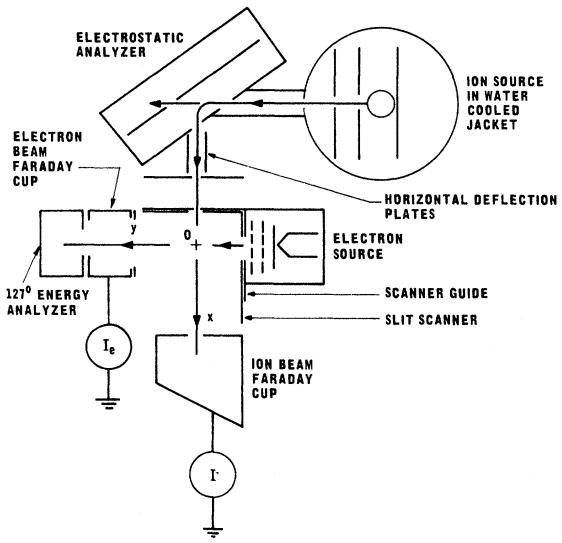

FIG. 2. Schematic diagram of experimental apparatus.

four-inch diffusion pump, a water cooled chevron baffle and a zeolite molecular sieve trap. No cryogenic trapping is employed in the vacuum system. Details of the vacuum system are contained in the Ph. D. Thesis of W. C. Lineberger[13] and will not be repeated here.

B. Ion Beam Source and Optics

Three types of ion sources were considered for this experiment: the electron bombardment source, thermionic source, and surface ionization source. The electron bombardment source was eliminated because of the uncertainiy in the state of excitation of the emerging ion beam, for example, the metastable 5^2D levels of Ba^+ might be excited.

Initially, attempts were made to develop a thermionic source of barium ions similar to others reported in the literature. Because of insufficient current intensities and source lifetime, this type of source was abandoned.

Surface ionization proved to be a satisfactory method of obtaining an ion beam of the order of 10^{-7} A with a lifetime of the order of weeks and operable in an ultra high vacuum chamber. The final version of this source, shown in Fig. 3, utilizes surface ionization of neutral barium on a hot rhenium filament. Barium metal is evaporated from a molybdenum crucible which is heated to approximately 600 °C by a tungsten filament electrically insulated from the crucible by a thin coating of alumina. The crucible is $\frac{3}{8}$ in. o.d., $\frac{1}{4}$ in. i.d. by 1 in. long. The rhenium filament, with dimensions of 0.002 in. $\times \frac{1}{8}$ in. $\times$ 1 in., is secured at both ends in iron clamps which serve as electrical connections and mechanical supports. The filament is heated to approximately 1800 °C by a direct current of 15 to 18A. The barium gas diffuses into the region around the filament through a $\frac{1}{8}$ in. diameter hole in one of the end plates; this plate offers thermal isolation between the crucible and the filament. This thermal isolation is necessary to maintain the crucible of barium at the desired temperature and hence maintain the desired rate of evaporation. Around the filament is a molybdenum tube of 0.003 in. wall thickness with a $\frac{1}{16}$ in. $\times \frac{3}{4}$ in. slit through which the ionized barium is extracted. The ionizing filament is held at the desired positive acceleration potential of the beam while the extraction electrode is biased negatively approximately 50 V with respect to the filament. This bias is used to control the intensity of the ion beam. The exit electrode is held at ground potential while the repeller electrode is maintained at the acceleration potential. An ion current of the order of 10^{-7} A is obtained at an acceleration potential of 500 to 1000 V.

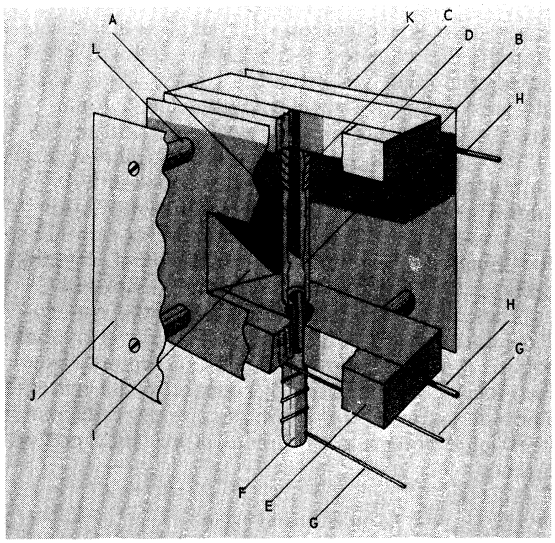

(A) SURFACE IONIZATION FILAMENT
(B) MOLYBDENUM SLEEVE (WITH SLIT)
(C) ALUMINA SLEEVE
(D) UPPER CLAMP FOR FILAMENT
(E) LOWER CLAMP FOR FILAMENT
(F) MOLYBDENUM CRUCIBLE
(G) CRUCIBLE HEATER
(H) CURRENT LEADS FOR FILAMENT
(I) EXTRACTION ELECTRODE
(J) EXIT ELECTRODE
(K) REPELLER ELECTRODE
(L) INSULATING SPACER

FIG. 3. Surface ionization source for barium ions.

The ion beam was mass analyzed on a magnetic sector mass spectrometer and, after about 12 hours of operation, barium ions constituted more than 99.9% of the total emission. Since the beam contamination contributes nothing to the signal, the only error introduced by the contamination is in the measurement of the barium ion beam current.

The possibility of the ion beam being metastably excited must be considered because the energy levels of the $5^2D_{3/2}$ and the $5^2D_{5/2}$ states lie only 0.6 and 0.7 eV, respectively, above the $6^2S_{1/2}$ ground-state level. If the ions achieve thermal equilibrium with the surface of the ionizing filament at a temperature of 2100 °K, then, from Boltzmann statistics, 7% of the beam would be excited to the $5^2D_{3/2}$ state and 6% of the beam would be excited to the $5^2D_{5/2}$ state. The spontaneous emission transition probabilities for the $5^2D_{3/2} \rightarrow 6^2S_{1/2}$ and the $5^2D_{5/2} \rightarrow 6^2S_{1/2}$ transitions have been calculated[14] to be 0.014 and 0.030 sec^{-1}. Assuming the ions are in the radiation field of a 2100°K blackbody and using the above emission transition probabilities, the transition probabilities for the $6^2S_{1/2} \rightarrow 5^2D_{3/2}$ and the $6^2S_{1/2} \rightarrow 5^2D_{5/2}$ transitions are 0.001 and 0.002 sec^{-1}, respectively. The extraction field of the ion source, of the order of 1 V/cm, extracts the ion from the source in approximately 10^{-5} sec. The length of time that the ion remains in the source is therefore insufficient for the ion to reach thermal equilibrium with the rhenium filament or to become metastably excited by radiation adsorption. The voltage drop across the rhenium filament, approximately 5 V, is too small to cause any metastable excitation problems by electron impact. The ion beam is considered, therefore, to be in the ground state.

The ion source is enclosed inside a water cooled jacket which is located inside the ultra high vacuum chamber. After the ion beam emerges from the source, it passes through a parallel plate electro-

static analyzer[15] which serves as a neutral particle and photon trap. Exiting the analyzer, the beam passes through parallel plate horizontal and vertical deflection structures used for pulsing and steering the beam. Aperture plates are placed between the analyzer and the interaction region to collimate the beam to dimensions of approximately 3 mm wide by 1 cm high.

As seen in the schematic diagram in Fig. 2, the ion Faraday cup is a deep cup with the surface being struck by the ion beam inclined with respect to the beam. The solid angle subtended by the entrance to the cup at the region where the ion beam strikes the cup is less than 1% of the total solid angle. In addition, secondary electron and reflected ion suppression structures are incorporated into the cup, but it has been demonstrated that the cup is essentially 100% efficient in retaining reflected and secondary charged particles, even when no voltages are applied to the suppression electrodes. Under operating conditions with both the ion and electron beams on, an electron current, of the order of several per cent of the ion beam current, was striking the ion Faraday cup. This current, a negligible fraction of the total electron beam current, was partially composed of "cold" electrons and partially energetic electrons with the energy of the electron beam. To eliminate this stray electron current, the ion cup was held at a potential of – 120 V. At this potential, secondary electrons were ejected from the cup. This problem was eliminated by placing the suppressor electrode in the cup at – 300 V. At these potentials, it was demonstrated that the cup was collecting all the ion beam current while not picking up any stray electron current. To keep electric fields at the ion cup out of the interaction region, a plate at ground potential was placed between the ion cup and the interaction region. The aperture in this plate is larger than the entrance to the ion cup and large enough to ensure that none of the ions in the beam are intercepted prior to entering cup. Furthermore, optical alignment of the collimating apertures of the ion source showed that no ion could be intercepted by this plate.

The average value of the ion beam current was measured with a Keithley 417 Picoammeter. The accuracy of this instrumentation, periodically checked with a Gyra Model CS-57 current source, is better than ±2%. The indicated ion beam energy was set with a John Fluke Model 413D voltage supply with an accuracy of ±0.25%. This accuracy was periodically verified with a John Fluke Model 871A differential voltmeter. The actual ion beam energy is estimated to be within ±1% of the indicated energy; this allows for the voltage across the ionizing filament to be superimposed on the acceleration voltage.

C. Electron Source, Collector, and Energy Analyzer

The electron source is a modified 6L6GC beam power tube similar to the one used in earlier work.[9,13] The source produces a beam with a rectangular cross section which is 2 cm wide by 3 mm high. Details for operation of an oxide cathode in a demountable vacuum system and the oxide cathode activation procedure are given elsewhere.[13,16]

The electron beam is collected in a Faraday cup which has two electrodes parallel to the back of the cup and perpendicular to the direction of the electron beam. The first electrode is a nickel grid with 85% transmission; this grid is connected to the Faraday cup, and its purpose is to prevent any electric field at the second electrode from penetrating the interaction region. The second electrode is a stainless steel plate with an aperture through which part of the beam can pass. In line with this aperture is an aperture in the rear of the electron cup through which approximately 1% of the electron beam passes when no suppression voltage is applied to the second electrode of the Faraday cup. This sample of the electron beam, taken along the major axis of the beam, enters a 127° cylindrical electrostatic energy analyzer, where the energy distribution of the electron beam can be determined. With suppression voltage on the second electrode, the cup was shown to retain 100% of the collected electron beam. An aperture plate is placed in front of the electron cup; this is used to give an indication of the space charge divergence of the electron beam as it traverses the interaction region. During data collection, the current to this plate is only a few per cent of the total electron beam current and is included in the total beam current measurement.

To correctly measure the average value of the modulated electron beam current, the current from the Faraday cup was passed through a low pass filter to a precision 10-Ω resistor and a Keithley Model 149 Milli-Microvoltmeter. The accuracy of the electron current measurement, periodically checked with a Gyra Model CS-57 current source, is better than ±2%. The indicated electron energy was set with a John Fluke Model 413C voltage supply with an accuracy of ±0.25% for voltages which are multiples of 10 V. This accuracy was periodically checked with a John Fluke Model 871A differential voltmeter.

The electrostatic energy analyzer is similar to the improved version of the Hughes and Rojansky analyzer[17] described by Marmet and Kerwin.[18] This analyzer was used to measure the energy distribution of the electron beam and, in particular, to measure where the peak of the energy distribution occurred with respect to the indicated electron beam energy. An energy degradation of a few electron volts is typical of an oxide coated cathode.

D. Interaction Region

The interaction region was designed to provide a field free space for intersection of the ion and electron beams. The interaction region is defined by a T-shaped bracket to which the ion beam collimating structure and the electron source are secured and on which the movable slit scanner rides. The slit scanner should intercept the ion and electron beams as close to the interaction region as possible; in this experiment the scanner

intercepts the two beams approximately $\frac{3}{8}$ in. prior to their intersection. The slit height on the scanner is 0.020 in. The linear motion of the scanner is introduced by means of a metal bellows assembly positioned with a micrometer drive. The scanner was also built so the leading edge could be used to measure an integral current distribution. This distribution when differentiated should give the same results as the differential distribution measured directly with the slit. Errors, in addition to the possible errors associated with the differential scanning procedure, might be introduced with the numerical differentiation which requires taking differences of large numbers. Throughout the experiment the difference in the measured form factor using these two procedures was less than 2%. Form factors taken routinely with the differential method were reproducible to better than 1%. The error associated with the form factor measurement is estimated to be no larger than ±2%.

E. Detection System

The photon detection system consists of a set of lenses, a vacuum chamber window, interference filter and a photomultiplier tube housed in a thermoelectric cooler. The output of the tube is processed for counting with a preamplifier, amplifier and pulse height analyzer.

The lens system is shown in Fig. 4. The dimensions of the collision volume are approximately 3 mm wide by 2 cm long by 3 mm deep. The first lens focuses an image of the collision volume approximately 2.5 cm above the window. This lens is made from two plano-convex lenses having a 55.0 mm focal length and a 42.0 mm diameter.

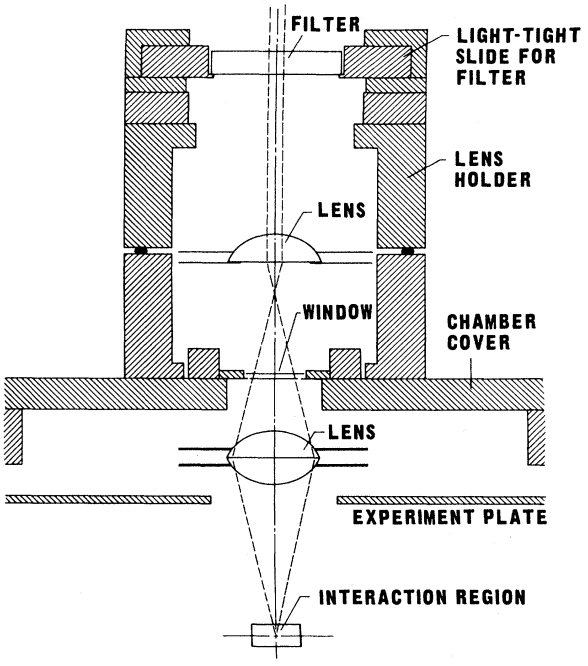

FIG. 4. Schematic diagram of lens system.

The window is a Granville-Phillips $1\frac{1}{2}$ in. diameter model with a 2 mm thick type-7056 Pyrex glass. The second lens is a single plano-convex lens identical to those described above. Its purpose is to collimate the light from the image of the collision volume so that it passes perpendicularly through the face of the interference filter. The filter, made by Thin Film Products, Inc., has a full width at half maximum of approximately 50 Å, a full width at 1% transmission of approximately 175 Å, and a peak transmission of over 60%. The transmission characteristics of each filter were measured over the range of 3000 to 6000 Å to check for spurious transmission peaks. The transmission outside a 600 Å passband was found to be less than 0.5%; thus the filter for one resonance line rejects the other resonance line by a factor of over 10^3. To facilitate interchanging filters, a light-tight slide[19] is used to hold the filters in place. The housing for the photomultiplier tube is located above the light-tight slide with the photocathode approximately 14 cm above the filter.

The output of the photomultiplier tube, an EMI 9584S, is processed for counting with an RIDL Model 10-17 preamplifier and an RIDL Model 33-13A counter–pulse-height analyzer combination. The counts are registered in an RIDL Model 49-25 timer-scaler. Because the signal and noise originate from similar sources the pulse-height distributions of the two are identical. For this reason, the analyzer is operated in an integral mode with the threshold set at the sensitivity level.

F. Beam Modulation System

The signal-to-noise ratio S/N, the stability of the signal and noise, and the sources of noise are parameters to evaluate in choosing a particular modulation scheme. For example, if S/N is large enough and both the signal and noise are sufficiently stable, no modulation is necessary and the experiment may be run with continuous beams. If modulation is necessary and if the magnitude of the noise from one beam is negligible compared to the signal, then the low-noise beam is the only beam that need be modulated, provided modulation does not introduce errors in the evaluation of the signal or noise. If the noise from both beams is comparable in magnitude with the signal and depends upon certain operating conditions, then double beam modulation is necessary. This latter case is discussed in more detail in the remainder of this section since it applies to the present experiment.

The sources of noise which led to the choice of the modulation scheme used in this experiment were:

1. A significant fraction of the residual gas in the vacuum chamber was neutral barium which escaped from the ion source. Upon impact by electrons, some of the barium was ionized and excited, thus producing photons against which the interference filters did not discriminate. This noise, N_e, was in phase with the electron beam and was a function of the electron beam current and energy as well as the barium partial

pressure.

2. Noise in phase with the ion beam N_i was produced when the projectile ion collided with the background gas. These collisions could produce noise photons by exciting the projectile ion or by ionizing and exciting the neutral barium as discussed above.

3. Light from the ion and electron sources was also a source of noise photons. The light from the ion source was reduced to a satisfactory level by shielding and by use of baffles. Necessarily, the electron source is near the interaction region. This resulted in a source of noise that could never be eliminated but was significantly reduced by collimation around the detector and by a reduction of the operating temperature of the source cathode consistent with good performance.

4. Light leakage around the detector was a source of noise that was virtually eliminated by proper optical shielding.

5. Thermal noise at the photocathode of the photomultiplier tube was satisfactorily reduced by cooling the tube to approximately -20°C in a thermoelectric cooler.

The background noise N_b is a sum of all the noises given in (3), (4), and (5) above. Of the background noise, approximately 85% can be attributed to light from the electron source; the remaining 15% comes from the ion source and the noise sources of (4) and (5) above.

Typical noise count distributions are listed in Table I. N_b was determined by counting for a period of 15 minutes with both the electron beam and the ion beam off. N_e was determined by counting for 15 minutes with only the electron beam on and subtracting N_b from the final count. Similarly, N_i was determined with only the ion beam on.

At a pressure of 5×10^{-9} Torr, turning off the ion beam resulted in a 10% drop in indicated pressure, while turning off the electron beam resulted in a 2% drop in pressure. If the experiment were run in a continuous beam mode, these pressure changes would give a 10% error in the measurement of N_e and a 2% error in N_i. If S/N were 10^{-1}, these errors could lead to as much as a 25% error in the measurement of the signal. Because of these errors introduced by pressure modulation, it was necessary to modulate both beams such that the period of modulation of both beams was short compared to the pressure time constant of the chamber, i.e.

$$\tau_m \ll V/S\,, \tag{9}$$

where S is the pumping speed, V is the volume of the vacuum chamber, and τ_m is the modulation period. The pressure time constant for the vacuum system used in this experiment is approximately 0.1 sec. The modulation period was varied from 4 to 32 msec. As will be shown later, the modulation criterion of Eq. (9) is sometimes not adequate to overcome pressure modulation in a volume of the size of the beam interaction region.

Basically, the modulation scheme is to square-wave modulate or chop both beams, and switch the output of the photomultiplier tube between two scalers in phase with the modulation signal, so that the signal plus noise is registered in one scaler, while the noise is registered in the other scaler. This is shown schematically in Fig. 5.

An examination of Table I shows that the noise of the electron beam N_e is the largest source of beam-dependent noise. Any error in evaluating this noise will reflect as a much larger error in the signal. Fortunately, N_i is relatively small and is not as difficult to evaluate as N_e. To ensure that the signal-plus-noise scaler registers the same N_e as does the noise scaler, the electron beam is modulated so that both scalers operate under identical beam configurations. This is achieved by chopping the electron beam at twice the frequency of the ion beam. The electron beam can then be on during either the first half of the "on" cycle of the ion beam, or it can be on during the second half. This phase parameter on the electron beam was alternated throughout the experiment so that any asymmetry in the ion beam was averaged out. With this arrangement, the signal-plus-noise scaler is on when both beams

TABLE I. Typical noise count distributions at three different electron energies. N_e—electron beam noise, N_i—ion beam noise, N_b—background noise, N_T—total noise count to "noise" scaler during a 15-minute counting period, $N_T = N_e + N_i + N_b$.

	20 eV	50 eV	100 eV	20 eV	50 eV	100 eV
	(a) As a function of pressure; $\lambda = 4554$ Å					
	Pressure: 2×10^{-8} Torr			Pressure: 7×10^{-9} Torr		
N_e	15%	57%	63%	3%	10%	24%
N_i	5%	3%	3%	3%	3%	2%
N_b	80%	40%	34%	94%	87%	74%
N_T	38,000	75,000	88,000	36,000	40,000	42,000
	(b) As a function of wavelength λ					
	$\lambda = 4934$ Å			$\lambda = 4554$ Å		
N_e	1%	4%	7%	3%	10%	24%
N_i	1%	1%	1%	3%	37%	2%
N_b	98%	95%	92%	94%	87%	74%
N_T	81,000	85,000	88,000	36,000	40,000	42,000

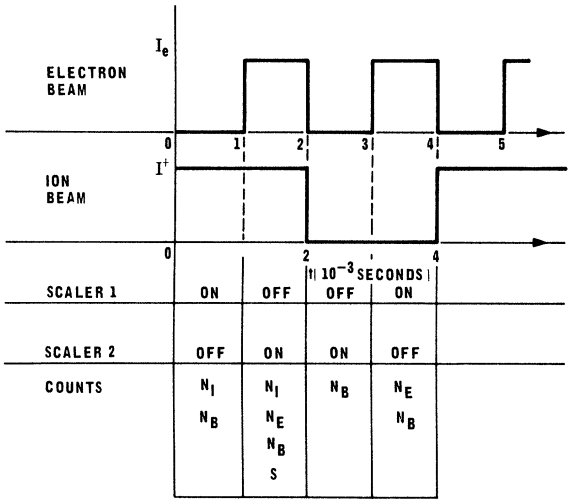

FIG. 5. Schematic diagram of beam pulsing sequence.

are on or both beams off; the noise scaler is on when only one beam is on.

The principal requirements of the pulsing apparatus are that the pulses have 50% duty cycles, stable pulse widths which are variable from one to ten msec, and rise times of the order of 10^{-3} times the pulse width. These specifications, plus the requirement of having both beams switch simultaneously, are met with the pulsing apparatus shown in Fig. 6. The ion beam was modulated at the horizontal deflection plates rather than the extraction plate of the ion source because of the high leakage current that occurred at the extraction plate due to barium deposited on the insulators.

As shown in Figs. 5 and 6, scaler 1 registers the noise, while scaler 2 registers the signal-plus-noise. The difference between the two scalers is therefore the signal S within the statistics of the counting process.

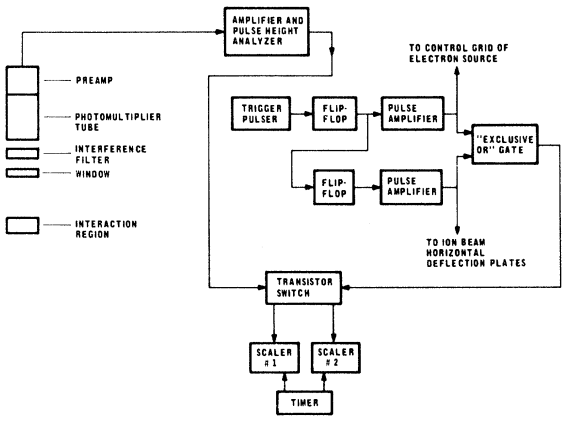

FIG. 6. Block diagram of pulse counting and beam modulating equipment.

G. Linear Polarizer

The polarization fraction was determined by orienting the axis of a linear polarizer first parallel to the electron beam and then perpendicular to the electron beam as discussed in Sec. II. A Bausch and Lomb type HN 32 linear polarizer with a luminous transmittance of 32% and an extinction transmittance of about 0.005% (two filters, axes crossed, transmit about 0.005%) was used in this experiment. To perform the measurement, the polarizer was placed in the light-tight slide just below the interference filter.

IV. EXPERIMENTAL PROCEDURES AND RESULTS

The experimental procedures and a demonstration that the apparatus performs in a manner consistent with the theory for the experiment are presented in this section, along with a discussion of the possible sources of error that are not implicit in the theory of the experiment.

A. Relative Emission Cross Section

The relative emission cross section in terms of the experimental parameters is given by

$$\sigma_{\mathrm{em}}{}^{R} \simeq (SF/I_i I_e)e^2 V_i \,. \tag{10}$$

The beam currents and velocities were straightforwardly determined with the apparatus described in the preceding section. After particular values for the currents and velocities were chosen, the form factor was measured using the slit scanner in the differential mode. Before the signal was measured, a counting period was established. For the majority of the measurements, T was chosen to be 15 min; this period resulted in a nominal relative error of $\pm 5\%$. In the latter stages of the data collection T was shortened to 5 min. After counting for a period of time T the signal was determined by taking the difference between the signal-plus-noise scaler and the noise scaler as discussed in the preceding section. After the phase of the electron beam modulation was changed by 180°, another counting period of length T was made; as mentioned in the previous section, the phase change on the electron beam modulation averages out any errors due to asymmetries in the ion beam. After four such counting periods, where the phase of the electron beam was alternated between each period, the electron beam was turned off and another count for a period T was determined. With the electron beam back on, four more signal counts similar to the first four were made. After these were completed, the ion beam was turned off and another count for a period T was made. Under proper operating conditions, the signal from the counting periods where the beams were off should be zero within the statistics of the counting process; these "beam off" conditions provided a running check on the symmetry of the pulsing apparatus. Over the entire data collection period, the "signal"

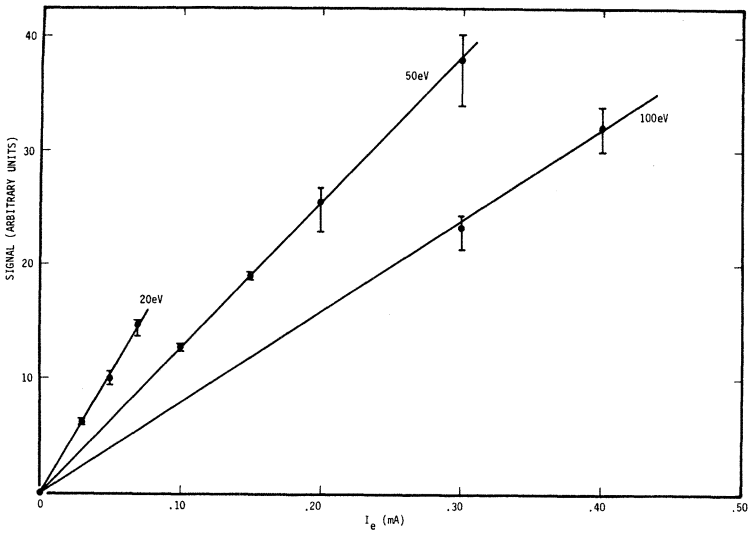

FIG. 7. Dependence of signal upon electron beam current I_e.

from the "beam off" operating conditions averaged to zero with no systematic deviation from zero.

From these eight periods of length T came eight sample values of the signal and eight sample values of the relative emission cross section. One data point for a given set of operating conditions and parameters is the average of a set of eight of these sample values. The beam pulsing frequency and the aperture plate current of the electron cup were recorded with each data run. The data were taken at randomly varied electron energies. In addition, the ion and electron beam intensities were periodically varied to assure that the measured cross sections were independent of these parameters.

1. *Consistency Checks*

A number of checks must be made before proper operation of the apparatus is assured. The results of the checks presented here pertain to the performance of the experimental apparatus during those periods in which the experimental results can be considered valid. The most obvious and necessary checks are planned variations of the experimental parameters in Eq. (10), which indicates that the signal should be linear with electron beam current and ion beam current and should intercept the origin. Figures 7 and 8 are graphs of signal versus electron beam current and ion beam current, which demonstrate the correct functional relationship. The error bars indicate the peak scatter in the experimental data.

Equation (10) also indicates that the signal should be linear with F^{-1}. Variation of F over a significant range of values in this experiment was not possible; the only variations which did occur were due to incidental changes in the ion beam profile. With these variations, F ranged from 0.95 to 1.20 and showed no systematic effect on the cross section. The electron beam is well contained inside the ion beam and the ion beam is relatively uniform over the region of the electron beam to ensure proper evaluation of F. A typical current distribution of the two beams is shown in Fig. 9. With such distributions, the form factor is a measure of the height of the ion beam along the Z-axis. (The "hump" at one end of the ion current distribution would tend to make F larger than the height of the ion beam.) If the height of the ion beam is changing as the beam traverses the interaction region, the measured value of F will be incorrect. Such changes in the ion beam can be introduced by passing the beam through an electrostatic lens system which causes the ion beam to either converge or diverge as it passes through the interaction region. To avoid such a possible error in this experiment, the height of the ion beam was collimated to approximately 1 cm rather than focused to this height with an electrostatic lens.

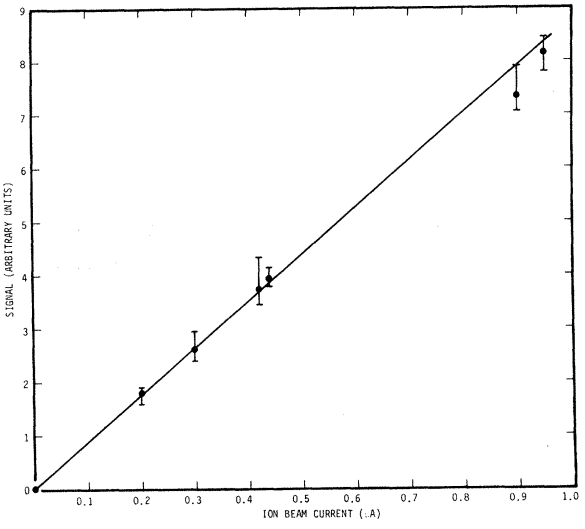

FIG. 8. Dependence of signal upon ion beam current I_i.

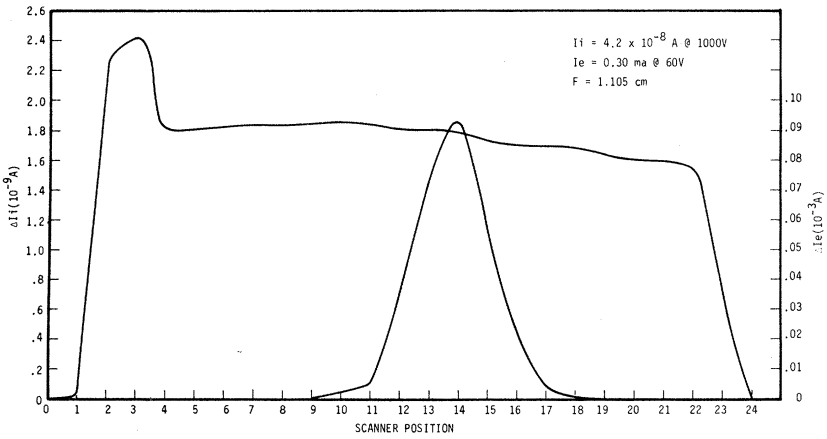

FIG. 9. Typical profile of ion and ion and electron beams. The electron beam is contained inside the ion beam.

The cross sections were also shown to be constant as the ion beam energy was varied from 500 to 1000 eV, and as the ion beam modulation period was varied from 4 to 32 msec.

2. *Possible Sources of Error*

This section deals with possible sources of error that cannot be detected by the systematic variation of the experimental parameters discussed in the preceding section.

Nonuniformly activated electron source. If the electron source is not uniformly activated or is partially poisoned along the length of its cathode, then this has the effect of changing the collision volume from a uniform distribution of photons to a nonuniform distribution. Since the photon detection probability is possibly not the same for each point in the collision volume, changes in the signal might occur if the collision volume changes. Because of the neutral barium residual gas in the chamber, the electron source cathode was highly activated, especially during the period immediately following bakeout, when the pressure remained high and the barium had not been adsorbed by the chamber walls. (Enhanced activation of an oxide cathode in the presence of barium at partial pressures of less than 5×10^{-9} Torr has been reported.[20]) The highly activated cathode was observed experimentally by the electron current at the electron cup being nearly equal to the total electron current leaving the cathode; i.e., only that portion of the cathode emitted electrons that was not "shadowed" from the residual barium gas. By turning off the power to the ion-source oven and allowing the crucible of barium to cool, the barium partial pressure would decrease and the above "highly activated" conditions on the electron source would disappear.

Under these highly activated conditions, the assumption was made that the electron source cathode was uniformly activated and the aperture plate current of the electron cup was recorded for several electron beam currents and energies. These aperture plate currents were established as a "standard" for a uniformly activated electron source cathode. In no case did an electron source produce a beam which gave a lower aperture plate current than that of the standard; however, some electron sources were rejected because they did not meet the specifications of the standard.

Unfortunately, the assumption of a uniform collision volume from an electron source that met the activation standard was never unequivocally proven despite the consistency of the results from several electron sources. However, this consistency of results indicates that the collision volume did not change enough during the measurements to introduce any detectable error in the measured relative cross sections.

Signal dependence upon electron beam position. Since the electron beam is contained inside the ion beam, the position of the collision volume with respect to the limiting aperture of the detection system is determined by the position of the electron beam and hence the position of the electron source. If the position of the electron beam changes when an electron source is replaced, an unnecessary systematic scatter in the data will occur, because the solid angle that the detection system subtends about the collision volume will change. To avoid this possible error, the electron beam maximum was maintained at scanner position number 14 as shown in Fig. 9.

Signal dependence upon electron beam noise. In determining the signal using the pulsing technique described in the previous section, the assumption is made that the magnitudes of the noise do not change under the different operating conditions. This assumption was found to be invalid. To discuss the problem, the following terms will be defined

1. $N_e(I_e, I_i)$ is the noise from the electron beam when both the electron beam and the ion beam are on.
2. $N_e(I_e, 0)$ is the noise from the electron beam when only the electron beam is on.
3. $N_i(I_e, I_i)$ is the noise from the ion beam when both the electron beam and the ion beam are on.
4. $N_i(0, I_i)$ is the noise from the ion beam when only the ion beam is on.

Referring to Fig. 5 the "noise" scaler or scaler 1 registers

$$C_1 = 2N_b + N_i(0, I_i) + N_e(I_e, 0)$$

and the "signal-plus-noise" scaler or scaler 2 registers

$$C_2 = S + 2N_b + N_i(I_e, I_i) + N_e(I_e, I_i).$$

In terms of these definitions, the assumptions are

(a) $N_e(I_e, I_i) = N_e(I_e, 0)$,

and (b) $N_i(I_e, I_i) = N_i(0, I_i)$,

so that $C_2 - C_1 = S$.

As discussed in the previous section, N_e is a function of the electron beam intensity and energy, and the barium partial pressure in the chamber, viz.,

$$N_e = \sigma_{ie} n_{Ba} (I_e/e) L \eta' , \tag{11}$$

where σ_{ie} is the cross section for ionization with excitation of barium by electron impact, n_{Ba} is the number density of neutral barium, I_e/e is the electron beam flux, L is the path length of the electron beam, and η' is the photon detection probability.

The experimental evidence that led to the discovery that assumption (a) was invalid, at least part of the time, was the fact that the indicated cross section increased as the pressure in the chamber decreased. This change in σ would take place only during the first two or three days after the chamber bakeout routine and was a function of the electron beam energy; at 20 eV there was no change, and at 50 eV the increase was less than the increase at 100 eV.

There was never any experimental evidence that assumption (b) was invalid; in fact, on the basis of the explanation of the error in assumption (a), it can be shown that assumption (b) is valid within the statistics of the present experiment. With this knowledge, the difference between scaler 2 and scaler 1 can accurately be given by

$$C_2 - C_1 = S + N_e(I_e, I_i) - N_e(I_e, 0) . \tag{12}$$

By plotting σ_{em} as a function of N_e/I_e, the error in assumption (a) may be deduced. Figure 10 shows that σ_{em} decreases as N_e/I_e increases. On the basis of Eq. (12), this implies that

$$N_e(I_e, I_i) < N_e(I_e, 0) , \tag{13}$$

for non-zero values of N_e/I_e.

The ion beam is modulated by modulating the voltage to one of the horizontal deflection plates with 0–50 V pulses. This alternately allows the ion beam to pass through the deflection plates to the interaction region or deflects the ion beam so that it does not pass through the interaction region. While the ion beam is "on" or passing through the interaction region, barium is adsorbed on the surfaces of the deflection plates and the surrounding collimation structures. When the ion beam is "off" or deflected out of the interaction region, barium is dislodged from the surfaces by ion impact causing the barium partial pressure to increase. The amount of barium hitting and sticking to the surfaces during the "on" portion of the cycle will be proportional to the barium partial pressure, and thus the amount of barium coming off the surfaces during the "off" portion of the cycle should also be proportional to the barium partial pressure. Hence, the degree that $N_e(I_e, I_i)$ is less than $N_e(I_e, 0)$ should be proportional to the barium partial pressure. This is reflected in Fig. 10 by σ_{em} decreasing as N_e/I_e increases.

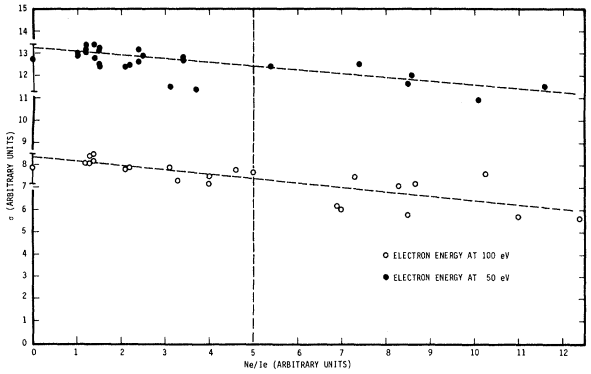

FIG. 10. Dependence of cross section upon N_e/I_e.

The dependence of the error in σ_{em} on the electron beam energy is explained by the energy dependence of σ_{ie}. At 20 eV the ratio σ_{ie}/σ_{em} is apparently much less than σ_{ie}/σ_{em} at 50 eV, which is in turn less than σ_{ie}/σ_{em} at 100 eV. Thus at 20 eV no change in σ_{em} within the statistics of the experiment could be detected, while at 50 eV a change in σ_{em} with pressure could be detected which was less than the change at 100 eV.

The fact that there was no apparent dependence of σ_{em} upon pressure at 20 eV is the "experimental evidence" mentioned above that assumption (b) is valid. That is, the pressure dependence error in σ_{em} is a function of electron beam parameters only and not a function of ion beam parameters. Furthermore, since N_i is much smaller in magnitude than N_e at higher pressures, any error in assumption (b) would be much more difficult to detect and, in this experiment, is less than the relative statistical error.

To plot the graph in Fig. 10, N_e was determined experimentally by taking the difference between the total count in the "noise" scaler when both beams were on, and the total count in the "noise" scaler when the electron beam was off. Thus N_e/I_e was determined for each data point that was measured. By plotting σ_{em} as a function of N_e/I_e and extrapolating to $N_e/I_e = 0$, the "true" value of σ_{em} should be found.

After each reassembly of the apparatus the 20, 50 and 100 eV data points of the 4554-Å line were remeasured as a check on the experimental apparatus. Because of this procedure, very little data at other energies and none on the 4934-Å line were taken in the higher N_e/I_e range. This lack of data at high N_e/I_e precluded the use of the extrapolation procedure to determine the "true" σ_{em}. Since no correction can be made on the measured values of σ_{em}, no data are included in the final averages when taken at $N_e/I_e > 5$ on the relative scale of Fig. 10 and a positive systematic error is added to the final average to allow for a

possible increase in the reported value of σ_{em}. The positive systematic error is energy dependent; from 10 to 39 eV there is no additional error, and at 100 eV there is a +6% systematic error. Table II gives the systematic error as a function of the indicated electron energy. These values of error were determined on the basis of the extrapolation in Fig. 10 where the average of the data taken at $N_e/I_e \leq 5$ is shown on the ordinate of the graph along with the peak scatter of the data included in the final average.

A better-cooled ion source and improved trapping of the neutral barium in the ion beam would eliminate this pressure dependent error in σ_{em}. The improved trapping could be achieved by cooling the back plate of the electrostatic analyzer.

B. Electron-Beam Energy Distribution

The electron-beam energy distribution was measured at 20, 50 and 100 eV using the procedure described in the previous section. Energy distributions were measured after each reassembly of the apparatus, and the measurements were reported periodically. The average full width at half maximum of the energy distribution is (1.5 ±0.5) eV; the energy distribution of the electron beam is therefore sufficiently narrow that no deconvolution of the data is necessary. The peak of the energy distribution occurs at a voltage below the indicated electron voltage; the average difference in these two voltages is (2 ± 1) V. To correct the data for this shift in the indicated electron energy, the actual electron energy was taken to be (2 ± 1) V below the indicated value.

C. Relative Cross-Section Data and Errors

The relative cross section data and errors are given in tabular form in Tables III and IV and in graphical form in Fig. 11. These data are the experimental data multiplied by a factor of 10^{20}. The random error given in the tables covers over 95% of the experimental data. The standard deviation and the 90% confidence limits[21] are included for comparison with other experimental presentations. The standard deviation is largely due to the Poisson statistics of the counting process. The systematic error is the sum of all the systematic errors discussed previously plus the pressure-dependent error given in Table II. The data presented here were taken over a period of three months, while the apparatus was assembled and disassembled seven different times. The data showed no systematic variation other than the systematic pressure dependence over this period of time.

TABLE II. Systematic error in $\sigma_{em}{}^R$ necessary to account for a possible pressure effect upon measurements.

Indicated electron energy (eV)	systematic error (%)
10–30	0
40	+1
50	+3
60	+3
70	+4
80	+4
90	+5
100	+6

D. Polarization Fraction

With the addition of the polarizing film, the procedure for measuring the polarization fraction was similar to the procedure for measuring the relative emission cross section. From eight 5-min counting periods an average value of $\phi_{\parallel}$ was determined when the axis of the polarizer was aligned parallel to the electron beam, and similarly, from eight 5-min periods an average value of $\phi_{\perp}$ was determined when the axis of the polarizer was perpendicular to the electron beam. The polarization fraction is given by

$$P = (\phi_{\parallel} - \phi_{\perp})/(\phi_{\parallel} + \phi_{\perp}) . \tag{14}$$

This procedure was repeated eight times at 20, 50 and 100 eV indicated electron energies for both the 4934-Å line and the 4554-Å line to determine an average value of P at each of these energies. The results of these measurements are presented in Table V along with the maximum scatter in the experimental data. A smooth curve drawn through a graphical presentation of these data and extrapolated to 10 eV indicates that the magnitude of the polarization is less than 15%; this value also encloses most of the experimental scatter. As indicated by Eq. (7), a 15% value for the polarization changes the measured cross section by 5%. Because of the small magnitude of the polarization data and the accompanying large experimental scatter, no attempt was made to correct the relative cross section for the polarization fraction. Instead, ±5% uncertainty was added to the relative emission cross section to allow for a possible ±15% polarization fraction.

E. Estimate of Photon Detection Probability

This experiment was initially designed without a lens system. The cross section for the 4554-Å line was measured at several electron energies using this design. However, when attempts to measure the cross section for the 4934-Å line were made, the scatter in the data was too high for satisfactory results because of a lower signal and a higher background noise. To overcome this problem, the present lens system was designed and installed.

With the no-lens system, the photocathode was collimated so that each point on the cathode could "see" every point in the collision volume. Hence, estimating the total solid angle that the photocathode subtended about the collision volume was a straightforward procedure. An estimate of the transmission of the interference filters and the windows on the vacuum chamber and in the cooling unit, and the quantum efficiency of the photomultiplier tube was available from the manufac-

TABLE III. Relative emission cross section data and errors for $6^2P_{1/2}^{\circ} \rightarrow 6^2S_{1/2}$. The random error encloses all data points except three out of a total of 93.

Indicated electron energy (eV)	Actual electron energy (eV)	σ_{em}	Standard deviation (%)	90% Confidence limits (%)	Random error (%)	Systematic error (%)	Total error (%)
10	8 ± 1	14.0	± 24	± 15	± 30	± 6	± 36
20	18 ± 1	9.6	± 7	± 4	± 20	± 6	± 26
30	28 ± 1	7.8	± 11	± 9	± 20	± 6	± 26
40	38 ± 1	6.8	± 5	± 3	± 20	$^{+7}_{-6}$	$^{+27}_{-26}$
50	48 ± 1	6.1	± 9	± 6	± 20	$^{+9}_{-6}$	$^{+29}_{-26}$
60	58 ± 1	5.6	± 13	± 7	± 20	$^{+9}_{-6}$	$^{+29}_{-26}$
70	68 ± 1	5.1	± 5	± 4	± 16	$^{+10}_{-6}$	$^{+26}_{-22}$
80	78 ± 1	4.6	± 8	± 5	± 16	$^{+10}_{-6}$	$^{+26}_{-22}$
90	88 ± 1	4.2	± 4	± 3	± 16	$^{+11}_{-6}$	$^{+27}_{-22}$
100	98 ± 1	3.9	± 10	± 5	± 16	$^{+12}_{-6}$	$^{+28}_{-22}$

turer of each item. From these estimates, an estimated photon detection probability for the no-lens-system was 1.7×10^{-5} at $\lambda = 4554$ Å and 1.6×10^{-5} at $\lambda = 4934$ Å. After the lens system was installed the signal increased by a factor of 8.2 giving an estimated overall detection probability of 1.4×10^{-4} at $\lambda = 4554$ Å and 1.3×10^{-4} at $\lambda = 4934$ Å. The estimated systematic error on these values is ±40%.

F. Estimated Absolute Cross Sections

The relative emission cross sections given in Tables III and IV are multiplied by a factor of 10^{+20} Taking this factor into consideration along with the estimated photon detection probability as shown by Eq. (7) gives the estimated absolute cross sections. These data are presented in Table VI. As discussed previously, a ±5% error

TABLE IV. Relative emission cross section data and errors for $6^2P_{3/2}^{\circ} \rightarrow 6^2S_{1/2}$. The random error encloses all data points except three out of a total of 109.

Indicated electron energy (eV)	Actual electron energy (eV)	σ_{em}	Standard deviation (%)	90% Confidence limits (%)	Random error (%)	Systematic error (%)	Total error (%)
10	8 ± 1	27.7	± 7	± 4	± 10	± 6	± 16
20	18 ± 1	20.3	± 4	± 2	± 10	± 6	± 16
30	28 ± 1	16.6	± 6	± 5	± 10	± 6	± 16
40	38 ± 1	14.3	± 5	± 3	± 10	$^{+7}_{-6}$	$^{+17}_{-16}$
50	48 ± 1	12.8	± 5	± 2	± 10	$^{+9}_{-6}$	$^{+19}_{-16}$
60	58 ± 1	11.7	± 5	± 3	± 10	$^{+9}_{-6}$	$^{+19}_{-16}$
70	68 ± 1	10.3	± 6	± 5	± 10	$^{+10}_{-6}$	$^{+20}_{-16}$
80	78 ± 1	9.7	± 5	± 4	± 10	$^{+10}_{-6}$	$^{+20}_{-16}$
90	88 ± 1	8.8	± 4	± 2	± 10	$^{+11}_{-6}$	$^{+21}_{-16}$
100	98 ± 1	7.9	± 5	± 3	± 10	$^{+12}_{-6}$	$^{+22}_{-16}$

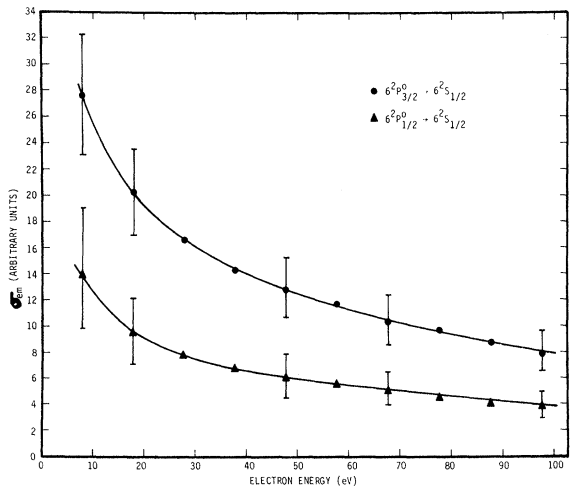

FIG. 11. Dependence of relative emission cross sections upon electron energy.

TABLE VI. Estimated absolute emission cross sections for excitation of the resonance transitions in Ba^+ ions by electron impact. The total error in the estimated absolute cross sections is the total error in the relative cross sections plus the ±5% error due to polarization plus the ±40% error in the estimated photon detection efficiency.

Actual Electron Energy (eV)	$\sigma_{em}(10^{-16}$ cm$^2)$ 4554 Å	4934 Å
8	19.8	10.8
18	14.5	7.4
28	11.9	6.0
38	10.2	5.2
48	9.1	4.7
58	8.4	4.3
68	7.4	3.9
78	6.9	3.5
88	6.3	3.2
98	5.6	3.0

is added to the estimated absolute cross sections to allow for a possible ± 15% polarization fraction.

V. COMPARISONS WITH THEORY

The general quantum mechanical treatment of excitation developed by Bethe[22] may be applied to the excitation of Ba^+ by electron impact. Using hydrogen-like wave functions and the Born approximation he has shown that at high electron energies the cross section for electron excitation of electric dipole transitions is given by

$$\sigma_{ex}(i \rightarrow j) = \frac{4\pi a_0^2 R^2 f_{ij}}{(E_j - E_i)E} \ln\left(\frac{CE}{E_j - E_i}\right), \quad (15)$$

where a_0 is the radius of the first Bohr orbit of the hydrogen atom, R is the Rydberg constant, E_i and E_j are the energies of the lower and upper levels, f_{ij} is the optical oscillator strength for the transition, E is the energy of the projectile electron, and C is a constant which must be evaluated for each atom or ion. In principle f_{ij} and C can be determined, but lack of accurate wave functions prevents this for most atoms or ions. Even without knowing these constants, the energy dependence of σ_{ex} at high electron energies is predicted to be

$$\sigma_{ex} = (A/E) + (B/E)\ln(E), \quad (16)$$

where A and B are constants. That the relative experimental data follow this energy dependence at high electron energies is shown in Fig. 12.

Seaton[23] has attempted to generalize Bethe's results to lower electron energies by introducing an empirical factor $\bar{g}$ so that

$$\sigma_{ex}(i \rightarrow j) = \frac{8\pi^2 a_0^2 R^2 f_{ij}}{3^{1/2}(E_j - E_i)E}\,\bar{g}, \quad (17)$$

TABLE V. Polarization fraction.

Indicated Electron Energy (eV)	Polarization Fraction (%)	Maximum Experimental Scatter
	$6^2P^o_{3/2} \rightarrow 6^2S_{1/2}$	
20	+3	±12
50	−3	± 5
100	−8	± 7
	$6^2P^o_{1/2} \rightarrow 6^2S_{1/2}$	
20	−3	±28
50	−3	± 6
100	0	± 8

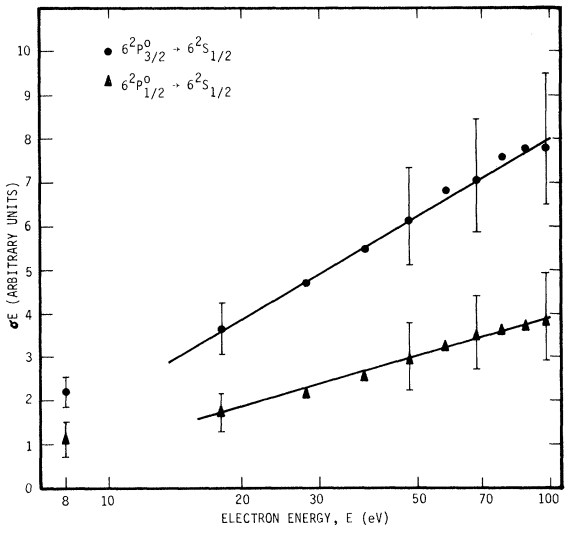

FIG. 12. Relative emission cross section times electron energy versus electron energy.

where, at high electron energies,

$$\bar{g} = (3^{1/2}/2\pi)\ln[E/(E_j - E_i)]. \quad (18)$$

At low and intermediate energies $\bar{g}$ is empirically evaluated with calculated and measured excitation cross sections. This empirical factor is tabulated by Van Regemorter[24] and also by Allen.[25] For strong allowed transitions, the strong coupling effects reduce the cross section by a factor of the order of two near threshold.[24,26] At high energies the accuracy may be expected to decrease as increasing departure from the one-electron atom is introduced. Using the experimental values of the oscillator strengths for Ba^+ obtained by Gallagher,[3] the cross section for the excitation of the 6^2P levels of Ba^+ has been calculated using Eq. (17). The results are presented in Fig. 13.

Another available theory for comparison with experimental results is the semi-classical collision theory of Gryzinski.[27] Calculations based on this theory, though directly applicable only to neutral targets, should approach the cross section for excitation of the ion at high electron energies where the coulomb field of the ion becomes negligible. Results of such a calculation are presented in Fig. 13. Notice that the ratio of the two cross sections at high electron energies is about 4.5, whereas, the ratio based on Seaton's theory is about two. When the energy difference between the two 6^2P levels is small compared to the electron energy, the ratio of the two cross sections should vary approximately as the ratio of the statistical weights of the two levels which, in this case, is two. Thus, in this respect, the calculations based on the theory of Gryzinski are incorrect although yielding results that are the same order of magnitude as those from Eq. (17).

To compare the experimental results with the theoretical predictions of the excitation cross section, the branching ratios and cascading effects must be included. The branching ratios for the $6^2P \rightarrow 5^2D$ transitions and the $6^2P \rightarrow 6^2S$ transitions have been experimentally determined by Gallagher[3] to be 0.26 and 0.74 within an accuracy of ± 10%. The only information on the cascading contribution to the emission cross section is that which can be inferred from the study of excitation of Cs, which is isoelectronic with Ba^+. In their experimental investigation of the excitation of Cs by electron impact, Zapesochnyi and Shimon[28] found that the cascade contribution to the resonance-line emission cross-section was approximately 10%. Assuming the resonance-line emission cross-section of Ba^+ contains the same relative cascading effects, and using the above values of the branching ratios, the theoretical values of the excitation cross section are converted to an emission cross section. In Fig. 14, the comparison is made between the results from the Seaton formula and the estimated absolute cross sections given in Table VI. The agreement between experiment and theory is remarkable considering the 60 to 80% error brackets on the experimental data and the 20% error brackets on the theoretical curve due to the experimental determination of the branching ratios, oscillator strengths, and cascading.

The general theory on polarization by Percival and Seaton[12] predicts a polarization value of 53% at threshold with a high energy limit of – 37% for

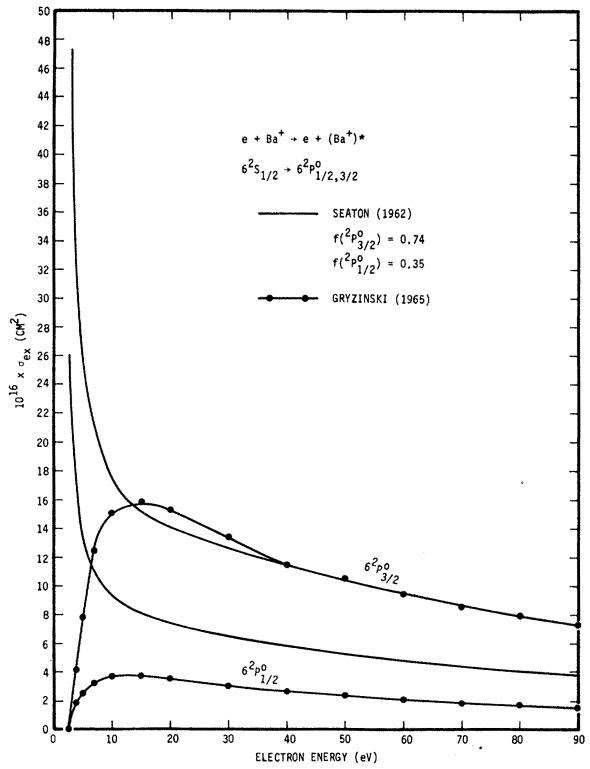

FIG. 13. Theoretical excitation cross sections versus electron energy.

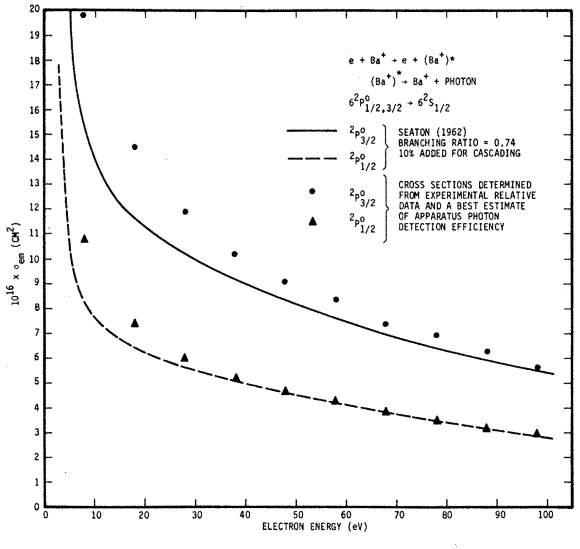

FIG. 14. Comparisons between estimated absolute emission cross sections and theoretical absolute emission cross sections.

the $Ba^+ 6^2P^\circ_{3/2} \rightarrow 6^2S_{1/2}$ transition and zero polarization for the $6^2P^\circ_{1/2} \rightarrow 6^2S_{1/2}$ transition. Qualitatively, the experimental data agree with these predictions; the data for the $6^2P^\circ_{3/2} \rightarrow 6^2S_{1/2}$ transition are positive at low energies and decrease to negative values at high energies, and the data for the $6^2P^\circ_{1/2} \rightarrow 6^2S_{1/2}$ transition are zero within the experimental scatter.

ACKNOWLEDGMENTS

We are pleased to acknowledge the expert assistance of R. K. Feeney and M. O. Pace during the developmental phases of the apparatus.

*This work was partially supported by the Controlled Thermonuclear Research Program of the U. S. Atomic Energy Commission.

†Present address: Sandia Laboratories, Albuquerque, New Mexico. This paper is based on a thesis submitted by F. M. B. to the faculty of the Georgia Institute of Technology in partial fulfillment of the requirements for the degree Doctor of Philosophy.

[1]F. M. Bacon, Ph.D. thesis, Georgia Institute of Technology, Atlanta, Georgia, 1968 (unpublished).

[2]C. Candler, Atomic Spectra (D. Van Nostrand Company, Inc., Princeton, New Jersey, 1964), p. 355.

[3]A. Gallagher, Phys. Rev. 157, 24 (1967).

[4]F. M. Bacon and J. W. Hooper, in Abstracts of Papers of the Fifth International Conference on the Physics of Electronic and Atomic Collisions, Leningrad, U. S. S. R., 17-23 July 1967 (Publishing House, Nauka, Leningrad, 1967), p. 41.

[5]A. R. Lee and N. P. Carleton, Phys. Letters 27A, 195 (1968).

[6]E. Hinnov, J. G. Hirschberg, F. W. Hofmann, and N. Rynn, Phys. Fluids 6, 1779 (1963);
N. Rynn, E. Hinnov, and L. C. Johnson, Bull. Am. Phys. Soc. 10, 213 (1965); and Rev. Sci. Instr. 38, 1378 (1967).

[7]K. T. Dolder, M. F. A. Harrison, and P. C. Thonemann, Proc. Roy. Soc. (London) A264, 367 (1961).

[8]M. F. A. Harrison, Brit. J. Appl. Phys. 17, 371 (1966).

[9]W. C. Lineberger, J. W. Hooper, and E. W. McDaniel, Phys. Rev. 141, 151 (1966); J. W. Hooper, W. C. Lineberger, and F. M. Bacon, Phys. Rev. 141, 165 (1966).

[10]G. H. Dunn and B. Van Zyl, Phys. Rev. 154, 40 (1967).

[11]D. F. Dance, M. F. A. Harrison, and A. C. H. Smith, Proc. Roy. Soc. (London) A290, 74 (1966).

[12]I. C. Percival and M. J. Seaton, Phil. Trans. Roy. Soc. London, Ser. A 251, 15 (1958).

[13]W. C. Lineberger, Ph.D. thesis, Georgia Institute of Technology, Atlanta, Georgia, 1965 (unpublished).

[14]R. H. Garstang and S. J. Hill, Publ. Astron. Soc. Pacific 78, 70 (1966).

[15]G. A. Harrower, Rev. Sci. Instr. 26, 850 (1955).

[16]F. Rosebury, Handbook of Electron Tube and Vacuum Techniques (Addison-Wesley Publishing Company, Inc., Reading, Mass., 1965), p. 98.

[17]A. L. Hughes and V. Rojansky, Phys. Rev. 34, 284 (1929);
A. L. Hughes and J. H. McMillen, Phys. Rev. 34, 291 (1929).

[18]P. Marmet and L. Kerwin, Can. J. Phys. 38, 787 (1960).

[19]E. C. Yates, Rev. Sci. Instr. 36, 1883 (1965).

[20]R. M. Matheson, L. S. Nergaard, and R. H. Plumlee, RCA Review 18, 385 (1957).

[21]J. S. Bendat and A. G. Piersol, Measurement and Analysis of Random Data (John Wiley & Sons, Inc., New York, 1966), p. 139.

[22]H. Bethe, Ann. Physik 5, 325 (1930).

[23]M. J. Seaton, Atomic and Molecular Processes, edited by D. R. Bates, (Academic Press, Inc., New York, 1962), Chap. 11.

[24]H. Van Regemorter, Astrophys. J. 136, 906 (1962).

[25]C. W. Allen, Astrophysical Quantities (The Athlone Press, University of London, London, 1963), 2nd ed., p. 42.

[26]H. Van Regemorter, Monthly Not. Roy. Astron. Soc. 121, 213 (1960).

[27]M. Gryzinski, Phys. Rev. 138, A305 (1965).
M. Gryzinski, Phys. Rev. 138, A322 (1965).

[28]I. P. Zapesochnyi and L. L. Shimon, Dokl. Akad. Nauk 166, 320 (1966) [English transl.: Soviet Phys. – Dokl. 11, 44 (1966)].

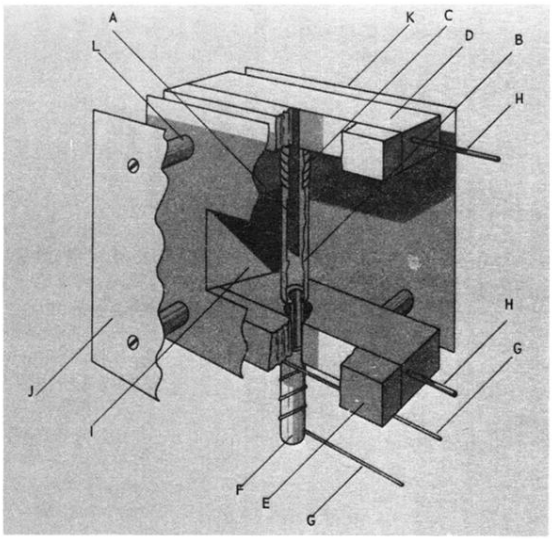

(A) SURFACE IONIZATION FILAMENT
(B) MOLYBDENUM SLEEVE (WITH SLIT)
(C) ALUMINA SLEEVE
(D) UPPER CLAMP FOR FILAMENT
(E) LOWER CLAMP FOR FILAMENT
(F) MOLYBDENUM CRUCIBLE
(G) CRUCIBLE HEATER
(H) CURRENT LEADS FOR FILAMENT
(I) EXTRACTION ELECTRODE
(J) EXIT ELECTRODE
(K) REPELLER ELECTRODE
(L) INSULATING SPACER

FIG. 3. Surface ionization source for barium ions.